Meteorologische Zeitschrift, Vol. **26**, No. 4, 421–430 (published online May 8, 2017)

Boundary-Layer Meteorology

Upper limit for wind shear in stably stratified conditions expressed in terms of a bulk Richardson number

Stefan Emeis*

Institute of Meteorology and Climate Research (IMK-IFU), Karlsruhe Institute of Technology (KIT), Garmisch-Partenkirchen, Germany

(Manuscript received September 21, 2016; in revised form March 15, 2017; accepted March 20, 2017)

Abstract

Profile measurements of wind and potential temperature from a land site (obtained by a RASS for several years) and an offshore site (obtained at the meteorological mast on the research platform FINO 1 for one year) are used to analyse the temporal evolution of wind speed and wind shear under statically stable conditions, especially in situations with low-level jets. In both cases a bulk Richardson number is calculated from the data. Data analysis indicates that there seems to exist a lower bound for the bulk Richardson number during stable stratification which is greater than zero. At this lower bound the flow reaches its maximum possible vertical wind shear. Even larger shear would then mean production of new turbulence which in turn would reduce the shear. Therefore, at this lower bound, the flow is in equilibrium between production and depletion of turbulence characterized by an equilibrium Richardson number. This equilibrium Richardson number is found here at about 0.1 for the land site and 0.04 for the marine site. For situations where maximum shear occurs, this shear can be compared to the shear described by the logarithmic vertical wind profile law for stable stratification. This allows the derivation of relations for the equilibrium Richardson number and the constant in the correction term of the logarithmic wind law in terms of the stratification parameter z/L_* and the surface roughness z_T for temperature.

Keywords: stable boundary layer, wind shear, low-level jet, Richardson number, wind profile law

1 Introduction

The analysis and prediction of the temporal evolution of wind speed and vertical wind shear in stably stratified atmospheric boundary layers (SBL) is important for long-range horizontal transport of pollutants (Banta et al., 1998) as well as for the electrical harvest from wind energy conversion (Emeis, 2012). In the absence of advection and breaking waves, surface friction and vertical wind shear in the SBL are the only turbulence generating mechanisms, counteracted by the stable temperature gradient (Caughey et al., 1979). This turbulence, e.g., rules the vertical mixing of trace substances in SBLs and is able to bring pollutants surviving in the residual layer down again to the surface (an example of this is the explanation of nocturnal secondary ozone maxima (Reitebuch et al., 2000)). Vertical shear and the related turbulence also have influence on the power curve of wind turbines (Elliot and Cadogan, 1990) and mean additional loads to wind turbines (Hansen and Larsen, 2005).

A prominent feature of SBL winds at land sites is the formation of nocturnal wind maxima which is frequently termed as "nocturnal low-level jets" (LLJ, Lettau, 1954; Blackadar, 1957). While the LLJ over land occurs in the time domain, a similar phenomenon can be observed in the space domain over near-coastal parts of the sea (Smedman et al., 1993), when warmer air from land flows offshore over colder water. Ideally, the formation of such jets is analytically described as a frictionless inertial oscillation (one oscillation is completed within one pendulum day) initiated by the sudden stabilisation of the surface layer after sunset or after passing the coastline. This oscillation exhibits a rapid wind speed increase in the first hours after the onset and then a continuous turning of the wind direction during the whole duration until the phenomenon is stopped by newly emerging thermal or frictional turbulence shortly after sunrise or after sufficiently long travel over sea. The maximum wind speed cannot be more than twice the geostrophic wind speed in this analytical model and this maximum speed should appear after about one third of a pendulum day (roughly seven hours, see, e.g., Wittich and Roth, 1984). Wittich and Roth (1984) already noted that observations do not perfectly fit to this conceptual model in seeing the maximum wind speed much earlier and in observing pulsating flow speeds afterwards.

Apart from the just mentioned jet phenomenon and from changes in large-scale synoptic forcing, wind speed increase with time in a SBL can have other causes as well. The diurnal variation of boundary layer thermal stability at land sites is sufficient to cause higher nocturnal wind speeds in a few hundred metres above ground while the wind speeds close to the ground decrease (see, e.g., Heald and Mahrt, 1981). This is suf-

*Corresponding author: Stefan Emeis, Institute of Meteorology and Climate Research (IMK-IFU), Karlsruhe Institute of Technology (KIT), Kreuzeckbahnstr. 19, 82467 Garmisch-Partenkirchen, Germany, e-mail: stefan.emeis@kit.edu

DOI 10.1127/metz/2017/0828

Gebrüder Borntraeger Science Publishers, Stuttgart, www.borntraeger-cramer.com

ficiently well described by the well-known logarithmic wind law together with the Dyer-Businger correction terms for atmospheric stability (Businger et al., 1971; Dyer, 1974). This diurnal stability variation transforms a nearly logarithmic daytime wind profile into a nearly linear nocturnal wind profile and vice versa while keeping the wind direction constant. Thus, detection of a LLJ should include the observation of a wind speed decrease above the jet in order to distinguish it from regular changes of the wind profile during the evening transition (for a detailed description of the evening transition see Mahrt, 1981a). On the other hand, for the assessment of pollutant transports or wind energy potentials just above the surface layer, it does not really matter whether the increase in wind speed and wind shear in the SBL is due to a jet formation or not. Much more interesting should be the question whether there is an upper limit to the vertical wind shear and thus to the wind speed at a given height.

Having found in an earlier study – in contrast to the abovementioned classical LLJ theory – that the nocturnal wind speed increase with time above the surface layer does not depend much on the geostrophic wind speed (Emeis, 2014), we want to make here a new attempt to analyse from measured data what could be the dominating factor which controls the magnitude of the wind speed increase and wind shear. A first attempt to do so was made by Wittich et al. (1986). They found from tower data that the nocturnal wind shear is depending on several parameters such as cooling rates, changes in turbulent kinetic energy, and geostrophic wind speed. For the dependence on geostrophic wind speed they found a slight decrease in shear until about 5 m/s and then a mild increase in shear of about 0.005 1/s per 1 m/s increase in geostrophic wind speed. A posteriori inspection of the data used in Emeis (2014) reveals a similar behaviour of the shear on the 850 hPa wind speed which had been interpreted as weak dependence on this wind speed in Emeis (2014).

According to the considerations mentioned above that the ratio between thermal damping and mechanical production of turbulence should be relevant for the state of turbulence and the vertical wind shear in a SBL, an analysis of the bulk Richardson number could be promising. Therefore, we are going to analyse here the relation between the wind shear and the bulk Richardson number in more detail. A simultaneous capture of wind and temperature profiles through a layer of several hundred metres depth with sufficient vertical resolution is necessary in order to perform such analyses. The operation of RASS (radio-acoustic sounding system) instrumentation (Emeis, 2010) is one option which offers such data. Data from the 100 m high FINO 1 mast in the North Sea 45 km off the German coast (Türk et al., 2008) could be likewise valuable for assessing similar processes (see, e.g., Smedman et al., 1993) in the marine boundary layer (FINO is the German abbreviation for "Forschung in Nord- und Ostsee" meaning Research in the North and Baltic Sea).

This study starts in Section 2 with some considerations why the bulk Richardson number could be a promising candidate for the description of the maximum wind shear in the SBL. Then Section 3 gives an overview over the used data before Section 4 presents an analysis of the relation between wind speed, wind shear increase and Richardson numbers from RASS (in the stable nocturnal boundary layer) and FINO 1 (in the stably stratified marine boundary layer) data. An analysis of the temporal variation of the bulk Richardson number from RASS data in the wind shear layer between 70 and 160 m above ground will elucidate the role of the Richardson number as a governing parameter for the nocturnal wind speed increase in this layer. Several years of data from RASS observations from a site north of Augsburg, Germany (Emeis et al., 2011) are analysed. The comparison of the evaluations from the RASS and FINO 1 data is made in order to see whether there are differences between inland and offshore conditions. Finally, a comparison to the logarithmic wind profile law is made.

2 Bulk Richardson number

There is an interesting conceptual difference between the classical LLJ theory and the logarithmic law with its stability corrections. The ideal LLJ theory (Blackadar, 1957) stipulates the absence of turbulence whilst the validity of the logarithmic wind law requires the presence of turbulence (Businger et al., 1971; Dyer ,1974). As nature nearly never is ideal, most probably a mixture of both phenomena occurs most times. Thus, turbulence is nearly always important when analysing and describing LLJ. While stable thermal stratification tends to suppress turbulence, wind shear tends to produce turbulence mechanically (e.g., Stull, 1988). The negative ratio of the buoyant turbulence production term (which is negative if it is damping) and the shear production term (which is always positive) forms a dimensionless number known as the Richardson number, Ri. Due to the sign convention, Ri is positive with stable stratification. The bulk gradient Richardson number, Ri_B is frequently used, because it is most easily extracted from mean profile data (easier than the other well-known similar stability parameter z/L_*, where L_* is the Obukhov length, which usually requires the measurement of turbulent fluxes):

$$Ri_B = \frac{g\Delta\Theta_v\Delta z}{\Theta_v(\Delta u)^2} \tag{2.1}$$

where g is gravity, Θ_v is virtual temperature, Δz is the height interval over which Ri_B is computed and u is streamwise velocity. As wind direction is not considered in this definition of the bulk Richardson number, eq. (2.1) and the further discussion in this paper only deals with the averaged wind speed shear (see Heald and Mahrt, 1981). A considerable hysteresis is observed when using the Richardson number as an indicator for the transition from turbulent to laminar flow and

vice versa. Turbulent flow becomes laminar when turbulence depletion is larger than production, i.e. $Ri_B > 1$. On the other hand, laminar flow becomes turbulent when Ri_B decreases below a critical value in the order of 0.25, because in the absence of turbulence, e.g., wave formation is needed first to produce new turbulence (e.g., Stull, 1988).

The Richardson number has been investigated as an interesting parameter in the evolution of the vertical wind shear in the SBL since decades. Mahrt et al. (1979) and Mahrt (1981b) gave first examples of the vertical profile of the Richardson number during LLJ events and the variation of the vertical distribution of this number during the night from experiments such as Wangara (Clarke et al., 1971) and simple numerical modelling. The vertical distribution of the different terms of the turbulence energy budget during a marine LLJ event over the Baltic has been analysed in Smedman et al. (1993) from aircraft measurements. More recently, Banta et al. (2006) provided newer additional information from surface-based remote sensing (wind) and data from 55 m and 116 m towers (temperature). These studies show that Ri_B is around 0.15 in the sub-jet layer. Brümmer and Schultze (2015) showed vertical profiles of Ri_B from data from a 280 m high tower for different types of inversions and found that Ri_B first increases and later decreases in the course of the vertical growth of the surface inversion as a result of the growing vertical wind shear. Such behaviour was not visible from the nocturnal variation displayed in a height-time cross-section in Mahrt (1981b), most probably because continuous vertical profile data were not available at that time.

All the above mentioned studies linked the LLJ core wind speed (and thus the vertical wind shear in the sub-jet layer) to external conditions and did not consider investigating how the LLJ core speed could be governed by the turbulence regime underneath the jet itself. Banta et al. (2006), e.g., ascribe the nearly linear profiles of wind speed and temperature in the sub-jet layer to larger-scale processes. Only Van de Wiel et al. (2010) have made a first step to integrate friction into the classical conceptual LLJ model. They keep the inertial oscillation in their description, but now formulated this oscillation around a friction-dependent equilibrium wind vector rather than around the geostrophic wind vector. Obviously, the approach of van de Wiel et al. (2010) has much in common with a much earlier approach of Holton (1967) for the low-level jet over the sloping Great Plains. But this approach does not give winds larger than twice the geostrophic wind speed. The vast literature on the sloped Great Plains jet phenomenon is summed up in Shapiro et al. (2016). Shapiro et al. suggest a combination of the Blackadar (1957) and the Holton (1967) approach.

A similar subject is the analysis of gravity-driven downslope flows of cold air. A large amount of studies on katabatic flows exist starting with the pioneering work of Prandtl in 1942. Recent papers which also take into account Richardson numbers have been published, e.g., by Grisogono (2003) or Grachev et al. (2016). Again, nearly no study concentrates on the vertical wind shear and the maximum speed of the katabatic flow. Grisogono and Axelsen (2012) are amongst the few who do. They report that the maximum speed of katabatic flows depends inversely on the slope whilst Prandtl's solution for the speed of the katabatic flow does not depend on slope.

3 Data

RASS measurements were performed at the northern edge of the city of Augsburg, Germany with interruptions from 2008 to 2014. From April 24, 2008 until January 11, 2011 the instrument was deployed on the grounds of a waste incinerator just south of the motorway no. 8 passing Augsburg; from May 29, 2013 until December 3, 2014 the instrument was located on the grounds of Augsburg Airport about 1500 m north of the same motorway. The distance between the two locations is about two kilometres. The temperature recording was not working properly from July 30, 2010 until March 10, 2014. All in all, records with meaningful temperature profile data were available for 684 days from May 2008 to May 2014. 117 LLJ events were identified in this dataset for which the 850 hPa wind speeds were retrieved manually from the data of the Munich (Oberschleissheim) radiosonde. LLJ wind speed maxima were identified in the same (subjective) way as in an earlier study for Hannover (Emeis, 2014). The identification scheme was kept in order to allow for a comparison with this earlier study. The Metek RASS used in this study is a so-called sodar-RASS or Doppler-RASS (Emeis, 2010) consisting of a three-antenna sodar and a two-antenna radar system. The sodar component emits beeps from all three antennas at an acoustic frequency of 1600 Hz in the sodar mode and sweeps around a centre frequency of 1077 Hz from the vertical pointing antenna in the RASS mode. Two of the acoustic antennas were tilted at 16 degrees zenith angle, the third acoustic antenna was pointing vertical. The acoustic signal propagation is observed by a two-antenna radar system (3.8 m diameter each) working continuously at 474 MHz with a power of 20 W. The emitting antenna is placed 2.5 m upstream of the sodar, the receiving antenna 2.5 m downstream. Data analysis provides wind and temperature profiles up to 540 m with 20 m height resolution and 10 min temporal resolution. Temperature measurements have an accuracy of about 0.3 K, wind measurements of about 0.2 m/s.

Offshore wind and temperature data are taken from the 10 min mean values recorded at the 100 m research mast FINO 1 in the German Bight at eight heights between 30 m and 100 m above sea level. Here we use 30 m and 90 m wind speed values from cup anemometers and 30 m and 100 m temperature values from Pt100 sensors (Neumann et al., 2004). Wind speed at 90 m has

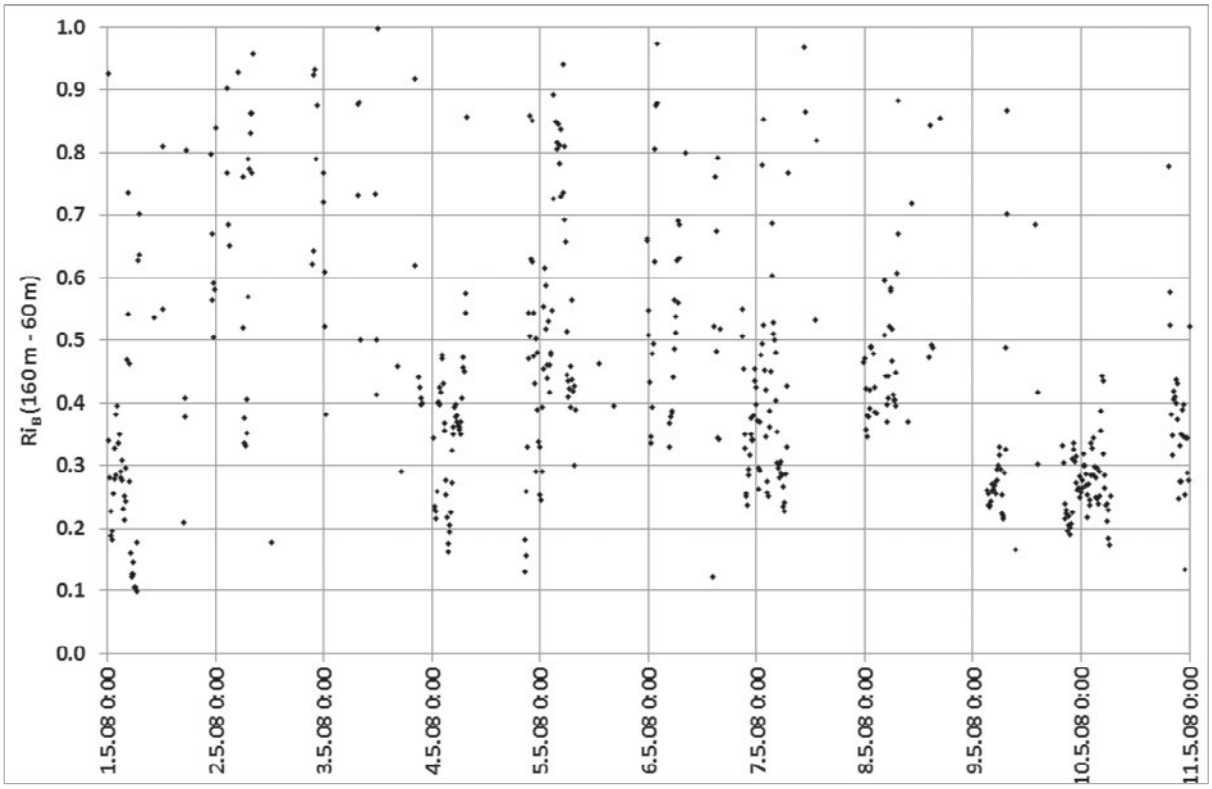

Figure 1: Moving 50 min average of bulk Richardson number for the first ten days in May 2008 at Augsburg, Germany from 10 min mean RASS wind and potential temperature data. Data has been evaluated for the layer 60 m to 160 m above ground. Vertical lines indicate midnight at time zone UTC+1. Only the stable range $0 < Ri_B < 1$ has been plotted.

been chosen, because the influence of the mast on 90 m data is probably quite similar to the influence on the 30 m data (whereas the mast-top anemometer at 100 m is the only instrument which is not influenced by the mast). Therefore, wind shear computed from the wind speed difference between 90 m and 30 m values should be more or less unaffected by the mast shadow. Temperature at 90 m is not available, therefore the nearest available data from 100 m has been used. Extensive evaluations of the FINO 1 data are described in Türk (2008). Türk (2008) has shown that potential temperatures at 30 m and 100 m are fairly equal for unstable conditions. These two temperatures are thus suited to compute a reliable bulk Richardson number.

4 Results

4.1 Inland wind shear and low-level jets

Profiles of wind and potential temperature data are used to calculate bulk Richardson numbers, Ri_B (see (2.1)). Fig. 1 shows Ri_B for ten days in May 2008 at Augsburg from RASS measurements of wind and potential temperature. Moving 50 min means of wind and temperature data at 60 m and 160 m above ground have been used to calculate Ri_B.

Only those data have been plotted in Fig. 1 which fall into the interval between $0 < Ri_B < 1$. Nighttime values are regularly in the range of Ri_B between 0.2 and 0.4. LLJs have been identified manually for the nights beginning on May 3, 4, 5, 7, and 9 with minimal Ri_B values down to 0.1. But similar small Ri_B values have been observed in the other nights as well.

Fig. 2 displays the temporal evolution of wind shear and Ri_B in the night from May 9 to May 10, 2008 in more detail by showing wind and temperature data as well. During daytime, i.e., before about 18 UTC+1, vertical gradients in wind speed and potential temperature are small due to thermally induced vertical mixing. Stabilisation of the atmospheric boundary layer starts shortly after 18 UTC+1 indicated by the spread between the two temperature curves in the upper part of Fig. 2. This temperature spread is immediately followed by the formation of a larger vertical wind shear as documented by the spread between the two wind speed curves in the lower part of Fig. 2. Following the temperature spread, strong stable conditions and wind shear last until about 8 UTC+1 on the next morning, although warming already started after sun rise shortly before 6 UTC+1. Slightly stable conditions persist until about 11 UTC+1.

The behaviour of Ri_B shows a large difference between daytime and night-time. Whilst Ri_B is heavily fluctuating during daytime, it is more or less constant at night-time at values mainly between 0.17 and 0.35 (see dots in Fig. 1 around midnight between May 9 and May 10 as well). This more or less constant behaviour even prevails when wind speed values change by a factor of 2 (see dips in wind speed shortly before midnight and

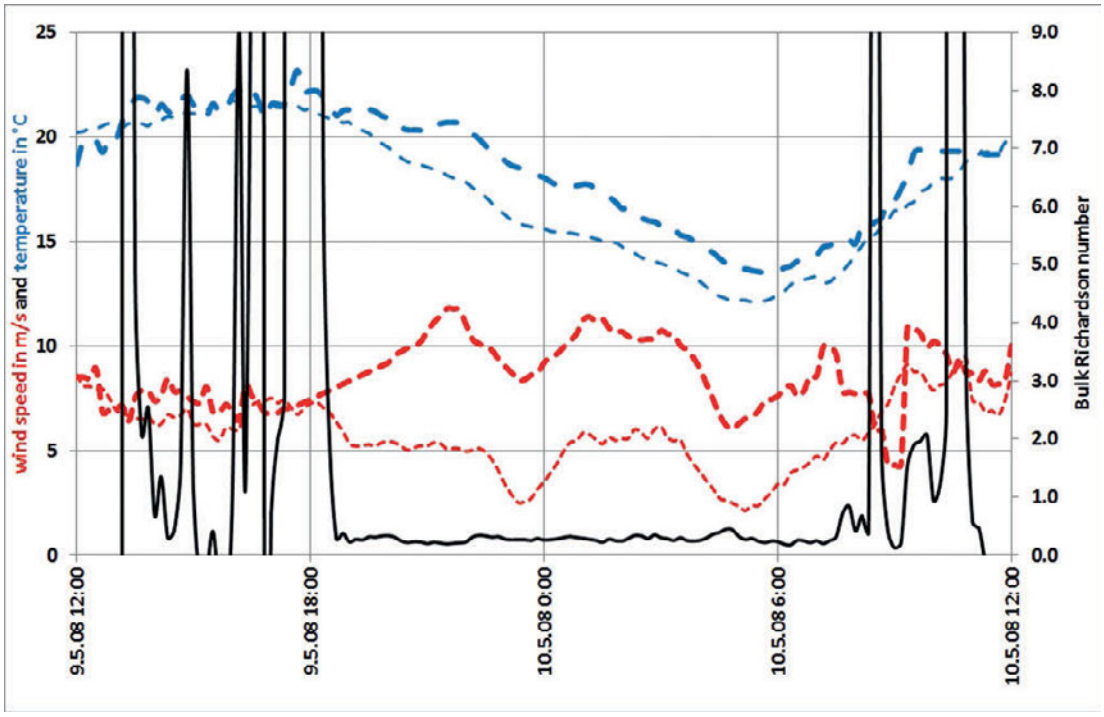

Figure 2: Moving 50 min mean of potential temperature (in °C (left axis), dashed blue lines), wind speed (in m/s (left axis), short dashed red lines), and bulk Richardson number (right axis, full line) at Augsburg, Germany for 24 hours from May 9, 2008 12 UTC+1 to May 10, 2008, 12 UTC+1. Bold lines: data from 160 m above ground, thin lines: data from 60 m above ground.

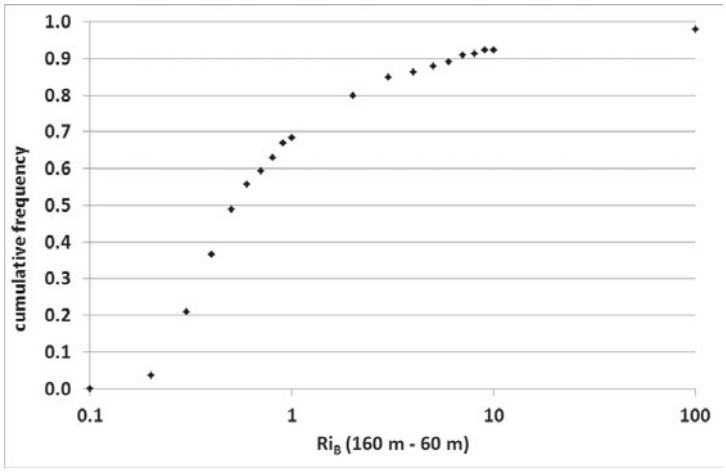

Figure 3: Cumulative frequency of Ri_B values for the ten days displayed in Fig. 1. The distribution covers the full range of all positive Ri_B values in contrast to Fig. 1. Note the logarithmic scale of the x-axis.

around sun rise in Fig. 2). Such behaviour is typical for many nights with LLJs. An analysis of the cumulative frequency distribution of the positive bulk Richardson numbers in the time period covered by Fig. 1 shows that nearly 70 % of all positive Ri_B values lie between 0.0 and 1.0 (Fig. 3).

Fig. 4 left displays the observed squared wind speed gradient per 100 m as function of the vertical potential temperature gradient per 100 m for 69 LLJ events at Augsburg within the period May 2008 and April 2010. The distribution of data points in Fig. 4 left seems to be bounded by two lines: (1) a lower limit at a squared wind speed gradient per 100 m of about 20 m^2s^{-2}, and (2) a limit to the upper left which can be interpreted by a limiting Richardson number. Therefore, Fig. 4 right shows the same data in a non-dimensional form using the bulk Richardson number Ri_B and the ratio between the maximum core wind speed in the LLJ and the 850 hPa

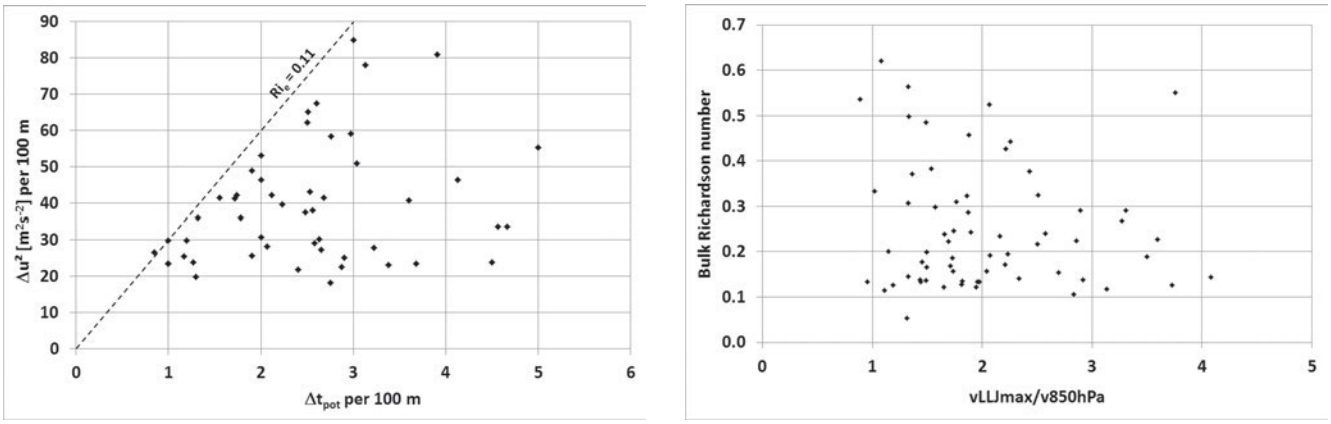

Figure 4: Left: Observed maximum squared wind speed gradient per 100 m versus observed vertical potential temperature gradient per 100 m for 69 low-level jet events at Augsburg which occurred between May 2008 and April 2010. The dashed line indicates $Ri_e = 0.11$. Right: Minimal 10 min mean bulk Richardson number (see eq. (2.1)) for the same events. Data have been determined for the 10 min interval within which the maximum LLJ wind speed was observed. The x-axis in the right-hand plot has been normalised by the 850 hPa wind speed from radiosonde observations in that night.

wind speed. The 850 hPa wind speed from midnight radiosonde ascents nearby (Munich Oberschleissheim) is used here as a proxy for the geostrophic wind speed during the nights with LLJ events. Again, as in Fig. 2, we find in Fig. 4 right a clear lower limit for Ri_Bin this distribution which is around 0.1 and which corresponds to the upper left limit in Fig. 4 left. This minimal value of Ri_B is henceforward called equilibrium (bulk) Richardson number and denoted by Ri_e. Data in Fig. 4 have been determined for the 10 min interval within which the maximum LLJ wind speed was observed (see Emeis, 2014). Fig. 4 right makes clear what had already been shown in Emeis (2014) that the LLJ core speed quite often exceeds twice the geostrophic wind speed, which is in contradiction to the classical LLJ theory.

4.2 Marine boundary layer example

In order to investigate whether the above shown findings for an inland site are a more general phenomenon, an example for offshore conditions has been evaluated in Fig. 5 using 10 min mean FINO 1 data for the entire year 2005. Like in Figs. 1 and 4 there is a region with no data close to $Ri_B = 0$ for $Ri_B > 0$. The lower bound Ri_e in the marine boundary layer seems to considerably lower (a bit less than 0.05) than in the inland boundary layer. Fig. 5 shows one similarity with Fig. 4 right: while there is large scatter for low wind speeds (or low wind speed ratios in Fig. 4 right), the Ri_B values approach the lower limit Ri_e for high wind speeds (or speed ratios in Fig. 4 right). Offshore high wind speed in the order of 20 m/s together with very low turbulence intensity normally occurs in weather conditions with warm air flowing from land out to the cold sea (see, e.g., Türk and Emeis, 2010 for such phenomena in the FINO 1 data). No geostrophic winds were available for this data set, thus the x-axis unfortunately could not be normalised in the same way as in Fig. 4.

5 Discussion

5.1 Low-level jet model

The observations shown in Figs. 1 to 4 allow for the following interpretation of the formation and persistence of nocturnal LLJs in seven steps which mediates between the two conflicting conceptual models (the frictionless LLJ model and the frictional logarithmic wind model):

1. after sun set the inland surface layer becomes stably stratified and turbulence dies out or is confined to smaller scales (which are no longer resolved by the present analysis, see Sun et al. (2016) for a discussion of this) in this layer (Ri_B becoming much larger than 1.0)
2. if a sufficient synoptic pressure gradient is prevailing, a LLJ starts to form at the top of this stably stratified surface layer
3. wind shear underneath the jet grows up to a certain value but not beyond (has also been shown in other publications such as, e.g., Banta et al., 2006)
4. maximal shear is reached when shear-generated turbulence production sets in underneath the jet core and produces enough friction to stop further wind acceleration
5. this finally leads to a new equilibrium of the nocturnal boundary layer flow at the maximum shear possible due to the given vertical temperature gradient (this maximum shear prevails and Ri_B stays at Ri_e for the rest of the night)
6. if sufficient large-scale forcing is present, the LLJ still continues to grow by developing jet cores at greater heights while keeping the (equilibrium) shear underneath its core constant (a positive correlation between jet core height and jet core speed has been observed in other studies, see, e.g., Emeis, 2014)

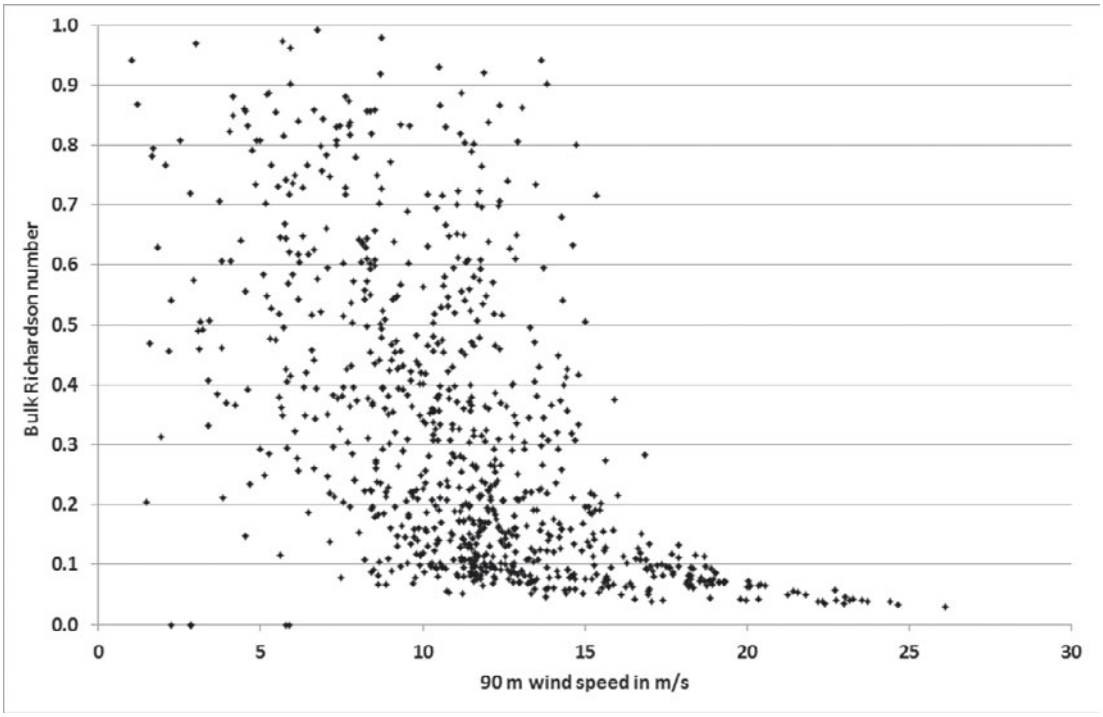

Figure 5: Bulk Richardson number in the marine boundary layer from 10 min mean data at FINO 1 for the year 2005. Wind speeds at 30 m and 90 m and temperature data at 30 m and 100 m have been used. Only Ri_B values for the interval $0 < Ri_B < 1$ are shown.

7. in nights with weak forcing the equilibrium described in step 5) is never reached and the observed Ri_B stays larger than the minimal bulk Richardson number, Ri_e.

This conceptual model can be applied to flows crossing ocean shore lines as well, if the time domain (distance from sun set) is substituted by a spatial domain (distance from the shore line). From a Lagrangian point of view, warm air crossing the shoreline towards a colder sea surface is equivalent to sun set: frictional forces disappear rapidly and the flow speeds up.

5.2 Difference between marine and inland boundary layers

An interesting difference seems to exist between the marine SBL and the nocturnal inland SBL. The minimal bulk Richardson number Ri_e in the marine boundary layer turns out to be considerably lower than in the inland boundary layer (0.04 instead of 0.1). The reason for this behaviour is not perfectly clear but may be found in the hysteresis already mentioned in Section 2. It needs some initialisation (e.g., wave formation) in order to create new turbulence in a SBL when Richardson numbers become lower again due to the increasing wind shear (stipulating a given constant vertical temperature gradient). This initialisation is more difficult over smooth ocean surfaces than over rough land surfaces. Therefore, a larger wind shear (and thus a smaller equilibrium bulk Richardson number Ri_e) is necessary to re-start production of turbulence in the marine boundary layer.

Before putting too much emphasis on this point, it should be kept in mind that Richardson numbers at Augsburg have been computed from remote sensing data whilst the numbers at FINO 1 have been derived from classical in situ instruments. Furthermore, the vertical height interval over which the bulk Richardson numbers have been computed at Augsburg is about twice as large as the one at FINO 1. Finally, the FINO 1 instruments at the two heights are separately calibrated instruments whilst the RASS at Augsburg does not need a calibration at all, because the determination of the temperatures at both heights are based on the same absolute physical relation between the sound speed and air temperature. On the other hand, as stated above, Türk (2008) has shown that potential temperatures at 30 m and 100 m are fairly equal for unstable conditions. This indicates that the calibration of these two instruments was equally good.

5.3 Comparison to the logarithmic wind profile law

The occurrence of an equilibrium Richardson number Ri_e which governs and limits the wind shear in the SBL offers an independent assessment of the wind profile law for the SBL.

Inverting Eq. (2.1) and making the assumption of the existence of an equilibrium Richardson number, Ri_e allows for the computation of the maximal nocturnal

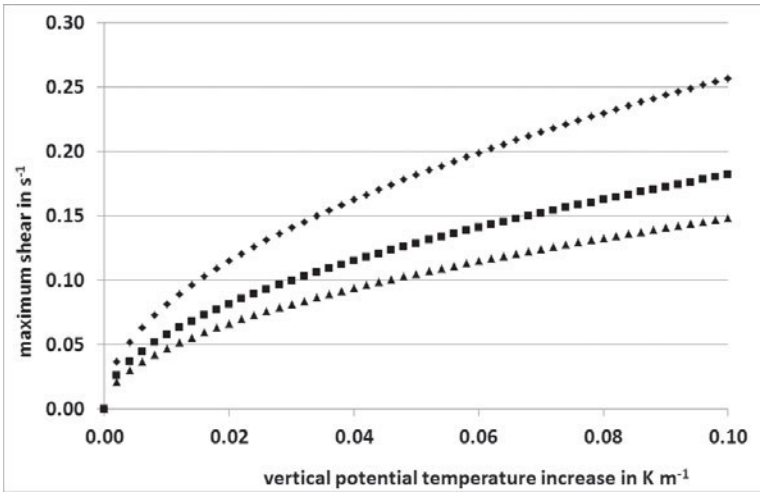

Figure 6: Maximum possible shear as a function of a given vertical temperature gradient in a SBL for different values of Ri_e (diamonds: 0.05, squares: 0.10, triangles: 0.15) using (5.1). The graphs in this Figure could likewise be interpreted as the minimum possible thermal stratification as function of a given vertical wind shear.

wind shear[1]:

$$\left(\frac{\Delta u}{\Delta z}\right)_{\max} = \sqrt{\frac{g\Delta\Theta_v}{\Theta_v \Delta z Ri_e}} \tag{5.1}$$

The resulting maximal possible shear from Eq. (5.1) as a function of a given vertical temperature gradient for different equilibrium Richardson numbers is displayed in Fig. 6. A similar plot presenting measured data can be found in Fig. 5 in Wittich et al. (1986).

Inserting finite differences into (5.1) over the height leads to a formula for the vertical wind profile:

$$u(z) = \sqrt{\frac{g}{\Theta_v Ri_e}} \sqrt{\frac{(\Theta(z) - \Theta(0))}{z}} z \tag{5.2}$$

where $u(z = 0)$ is set to 0.

The profile described by (5.2) can be compared to the usual logarithmic wind profile for stable stratification:

$$u(z) = \frac{u_*}{\kappa}\left(\ln\frac{z}{z_0} + a\frac{z}{L_*}\right) \tag{5.3}$$

where u_* is the friction velocity, z_0 is the roughness length, L_* is the Obukhov length, and a is a constant. For strong static stability with small values of the Obukhov length, the second term in the bracket of (4.3) is much larger than the first, logarithmic term and we get a nearly linear wind profile.

[1]The author agrees with one of the reviewers that the relation (2.1) could also be interpreted in the opposite way. Then – assuming the existence of an equilibrium bulk Richardson number Rie – (2.1) could be used to determine the minimal static thermal stratification possible for a given wind shear. Fig. 4 left and Fig. 6 could be used to do exactly this as well. But here, it is assumed that the radiative cooling of the surface is the driving force in a larger-scale synoptic regime with a given pressure gradient and geostrophic wind speed.

Equating (5.2) and the linear term in (5.3) sheds some light on the nature of Ri_e.

$$\sqrt{\frac{g}{\Theta_v Ri_e}} \sqrt{\frac{(\Theta(z) - \Theta(0))}{z}} z = \frac{u_*}{\kappa} a \frac{z}{L_*} \tag{5.4}$$

Equation (5.4) can be solved for Ri_e by using the usual definition of the Obukhov length, putting, $\kappa(\Theta(z) - \Theta(0)) = \Theta_* \ln\frac{z}{z_T}$ and $\overline{w'\Theta'} = u_*\Theta_*$ giving:

$$Ri_e = \frac{1}{a^2} \ln\frac{z}{z_T}\left(\frac{z}{L_*}\right)^{-1} \tag{5.5}$$

where z_T is the roughness length for temperature. (5.5) can only be a very rough estimation, because the used relations are mainly valid for a turbulent atmosphere. But two features are obvious. (1) Ri_e and z/L_* are inversely related, and (2) Ri_e depends on the surface roughness. Choosing $a = 5$ (Holtslag and de Bruin, 1988), $z_T = 0.1$ m, $z = 100$ m and $z/L_* = 2$ yields $Ri_e = 0.14$ which is not far from the observed value in the order of 0.1.

On the other hand, equating (5.2) and (5.3) can also be used to estimate the parameter a in the logarithmic wind law (5.3). This yields:

$$a = \left(\frac{z}{L_*}\right)^{-1} \frac{\kappa}{u_*} \sqrt{\frac{gz\Delta\Theta}{\Theta_v Ri_e}} = \sqrt{\frac{1}{Ri_e} \ln\frac{z}{z_T}\left(\frac{z}{L_*}\right)^{-1}} \tag{5.6}$$

where the first term on the right hand side comes from directly equating (5.2) and (5.3) and the term after the second equality sign comes from an inversion of (5.5). Choosing $z/L_* = 0.5$ (the upper value given in Holtslag and de Bruin for the validity of (5.3)), $k/u_* = 1.5$ s/m, $z = 100$ m, $\Delta\Theta/\Delta z = 0.07$ K/m, $\Theta_v = 290$ K and $Ri_e = 0.1$ yields $a = 4.6$ which is very close to the usual value.

5.4 Conclusions

This study was started in order to learn about which parameter best explains the maximum wind shear in a SBL. It is found that there exists a maximal wind shear underneath LLJs, the magnitude of which depends on the vertical temperature gradient in the sub-jet layer. This maximal shear is reached when a sufficiently large synoptic pressure gradient drives the flow. At this maximum, the flow reaches a new equilibrium between turbulence production by wind shear and turbulence depletion by static stability. This equilibrium can be characterized by an equilibrium Richardson number Ri_e. Inspection of wind time series showed that the equilibrium Richardson number Ri_e is relevant also for situations where we have a SBL without a distinct jet formation. These findings deviate from the classical frictionless LLJ theory.

Analysis of offshore wind and temperature data from the FINO 1 platform in the North Sea revealed a similar behaviour. Again, an equilibrium Richardson number Ri_e seems to exist which limits the maximal wind shear according to the existing vertical temperature gradient and which is reached in the case of a large synoptic pressure gradient. There are indications that the offshore equilibrium Richardson number is less than the inland one (about 0.04 instead of 0.1). Ri_e seems to depend on the surface roughness length (see (5.5)). It needs further investigations whether the difference between inland and offshore equilibrium Richardson numbers is real. Ri_e is not a universal constant, if the difference turns out to be real. Comparison to the logarithmic vertical wind profile law for stable stratification allows the derivation of relations for the equilibrium Richardson number and the constant in the correction term of the logarithmic wind law in terms of the stratification parameter z/L_* and the surface roughness z_T for temperature.

The next step could be to analyse in more detail why sometimes the equilibrium Richardson number is reached and sometimes not. This will hopefully explain the variability at lower wind speeds (wind speed ratios) in Figs. 1, 4, and 5, shown as vertical scatter. This could finally lead to wind profile laws for very stable conditions which circumvent the internal contradiction in the log-linear wind profile law where the frictional logarithmic law has to be corrected by a linear term in order to describe a smooth transition to nearly frictionless conditions.

Acknowledgments

The RASS instrumentation was operated and maintained by Carsten Jahn from IMK-IFU of KIT in Garmisch-Partenkirchen, Germany. The RASS measurements at Augsburg were financed from the basic funding of the institute (90 % from the German Federal Ministry of Education and Research (BMBF) and 10 % from the Federal State of Bavaria). The FINO data have been acquired in the framework of the research project OWID funded from 2005 to 2008 by the then German Federal Ministry of the Environment, Nature Conservation and Nuclear Safety (BMU) under grant no. 0329961. We acknowledge support by Deutsche Forschungsgemeinschaft and Open Access Publishing Fund of Karlsruhe Institute of Technology.

References

Banta, R.M., C.J. Senff, A.B. White, M. Trainer, R.T. McNider, R.J. Valente, S.D. Mayor, R.J. Alvarez, R.M. Hardest, D. Parrish, F.C. Fehsenfeld, 1998: Daytime buildup and nighttime transport of urban ozone in the boundary layer during a stagnation episode. – J. Geophys. Res. **103**, 22,519–22,544.

Banta, R.M., Y.L. Pichugina, W.A. Brewer, 2006: Turbulent velocity-variance profiles in the stable boundary layer generated by a nocturnal low-level jet. – J. Atmos. Sci. **63**, 2700–2719.

Blackadar, A.K., 1957: Boundary layer wind maxima and their significance for the growth of nocturnal inversions. – Bull. Amer. Meteor. Soc. **38**, 283–290.

Brümmer, B., M. Schultze, 2015: Analysis of a 7-year low-level temperature inversion data set measured at the 280 m high Hamburg weather mast. – Meteorol. Z. **24**, 481–494.

Businger, J.A., J.C. Wyngaard, Y. Izumi, E.F. Bradley, 1971: Flux profile relationships in the atmospheric surface layer. – J. Atmos. Sci. **28**, 181–189.

Caughey, S.J., J.C. Wyngaard, J.C. Kaimal, 1979: Turbulence in the Evolving Stable Boundary Layer. – J. Atmos. Sci. **36**, 1041–1052.

Clarke, R.H., A.J. Dyer, R.R. Brooks, D.G. Reid, A.J. Troup, 1971: 'The Wangara Experiment: Boundary-Layer Data'. – Technical Paper No. 19. Division of Meteorological Physics, CSIRO, Aspendale, Australia, 340 pp.

Dyer, A.J., 1974: A review of flux-profile relations. – Bound.-Layer. Meteor. **1**, 363–372.

Elliot, D.L., J.B. Cadogan, 1990: Effects of wind shear and turbulence on wind turbine power curves. – European Community Wind Energy Conference and Exhibition, Madrid, Spain, September 10–14, 1990. Available from http://www.osti.gov/scitech/servlets/purl/6348447 (read Aug. 4, 2016).

Emeis, S., 2010: Measurement Methods in Atmospheric Sciences. In situ and remote. Series: Quantifying the Environment Vol. 1. – Borntraeger Stuttgart. XIV, 257 pp.

Emeis, S., 2012: Wind Energy Meteorology – Atmospheric Physics for Wind Power Generation. Series: Green Energy and Technology. – Springer, Heidelberg etc., XIV, 196 pp.

Emeis, S., 2014: Wind speed and shear associated with low-level jets over Northern Germany. – Meteorol. Z. **23**, 295–304.

Emeis, S., K. Schäfer, C. Münkel, R. Friedl, P. Suppan, 2011: Evaluation of the interpretation of ceilometer data with RASS and radiosonde data. – Bound.-Layer Meteor. **143**, 25–35.

Grachev, A.A., L.S. Leo, S. Di Sabatino, H.J.S. Fernando, E.R. Pardyjak, C.W. Fairall, 2016: Structure of Turbulence in Katabatic Flows Below and Above the Wind-Speed Maximum. – Bound.-Layer Meteor. **159**, 469–494.

Grisogono, B., 2003: Post-onset behaviour of the pure katabatic flow. – Bound.-Layer Meteor. **107**, 157–175.

Grisogono, B., S.L. Axelsen, 2012: A Note on the Pure KatabaticWind Maximum over Gentle Slopes. – Bound.-Layer Meteor. **145**, 527–538.

Hansen, K.S., G.C. Larsen, 2005: Characterizing turbulence intensity for fatigue load analysis of wind turbines. – Wind Eng. **29**, 319–329.

Heald, R.C., L. Mahrt, 1981: The Dependence of Boundary-Layer Shear on Diurnal Variation of Stability. – J. Appl. Meteor. **20**, 859–867.

Holton, J.R., 1967: The diurnal boundary layer wind oscillation above sloping terrain. – Tellus, **19**, 199–205.

Holtslag, A.A.M., H.A.R. de Bruin, 1988: Applied modelling of the nighttime surface energy balance over land. – J. Appl. Meteor. **27**, 689–704.

Lettau, H., 1954: Graphs and Illustrations of Diverse Atmospheric States and Processes Observed During the Seventh Test Period of the Great Plains Turbulence Field Program. – Occasional Report 1, Atmospheric Analysis Laboratory, Air Force Cambridge Research Center, Mass.

Mahrt, L., 1981a: The early evening boundary layer transition. – Quart. J. Roy. Meteor. Soc. **107**, 329–343.

Mahrt, L., 1981b: Modelling the depth of the nocturnal boundary layer. – Bound.-Layer Meteor. **21**, 3–19.

Mahrt, L., R.C. Heald, D.H. Lenschow, B.B. Stankov, I. Troen, 1979: An observational study of the structure of the nocturnal boundary layer. – Bound.-Layer Meteor. **17**, 247–264.

Neumann, T., K. Nolopp, K. Herklotz, 2004: First Operating Experience with the FINO 1 Research Platform in the North Sea. – DEWI-Magazine **24**, 27–34.

Prandtl, L., 1942, Führer durch die Strömungslehre. – Vieweg und Sohn, Braunschweig, 373–375.

Reitebuch, O., A. Strassburger, S. Emeis, W. Kuttler, 2000: Nocturnal secondary ozone concentration maxima analysed by SODAR observations and surface measurements. – Atmos. Env. **34**, 4315–4329.

Shapiro, A, E. Fedorovich, S. Rahimi, 2016: A Unified Theory for the Great Plains Nocturnal Low-Level Jet. – J. Atmos. Sci. **73**, 3037–3057.

Smedman, A.-S., M. Tjernström, U. Högström, 1993: Analysis of the turbulent structure of a marine low-level jet. – Bound.-Layer Meteor. **66**, 105–126.

Stull, R., 1988: An Introduction to Boundary-Layer Meteorology. – Kluwer Academic Publishers, Dordrecht. 666 pp.

Sun, J., D.H. Lenschow, M.A. LeMone, L. Mahrt, 2016: The Role of Large-Coherent-Eddy Transport in the Atmospheric Surface Layer Based on CASES-99 Observations. – Bound.-Layer Meteor. **160**, 83–111.

Türk, M., 2008: Ermittlung designrelevanter Belastungsparameter für Offshore-Windkraftanlagen. – PhD thesis, Univ. of Cologne, 126 pp. http://kups.ub.uni-koeln.de/2799/

Türk, M., S. Emeis, 2010: The dependence of offshore turbulence on wind speed. – J. Wind Eng. Ind. Aerodyn. **98**, 466–471.

Türk, M., K. Grigutsch, S. Emeis, 2008: The Wind Profile Above the Sea – Investigations Basing on Four Years of FINO 1 Data. – DEWI Mag. **33**, 12–16. Available from http://www.dewi.de/dewi/fileadmin/pdf/publications/Magazin_33/03.pdf (read Aug. 4, 2016).

Van de Wiel, B.J.H., A.F. Moene, G.J. Steeneveld, P. Baas, F.C. Bosveld, A.A.M. Holtslag, 2010: A Conceptual View on Inertial Oscillations and Nocturnal Low-Level Jets. – J. Atmos. Sci. **67**, 2679–2689.

Wittich, K.-P., R. Roth, 1984: A case study of nocturnal wind and temperature profiles over the inhomogeneous terrain of Northern Germany with some considerations of turbulent fluxes. – Bound.-Layer Meteor. **28**, 169–186.

Wittich, K.-P., J. Hartmann, R. Roth, 1986: Analytical Shear Statistics Based on Nocturnal Wind Profiles. – J. Climate Appl. Meteor. **25**, 1507–1517.